Reversing-Pulse Electric Birefringence of Montmorillonite Particles Suspended in Aqueous Media.† Instrumentation and the Effect of Particle Concentration, Ionic Strength, and Valen...

ARTICLE *in* THE JOURNAL OF PHYSICAL CHEMISTRY · OCTOBER 1996

Impact Factor: 2.78 · DOI: 10.1021/jp961525+

3 AUTHORS, INCLUDING:

Ryo Sasai
Shimane University
119 PUBLICATIONS **1,314** CITATIONS

SEE PROFILE

THE JOURNAL OF PHYSICAL CHEMISTRY

Article

Reversing-Pulse Electric Birefringence of Montmorillonite Particles Suspended in Aqueous Media. Instrumentation and the Effect of Particle Concentration, Ionic Strength, and Valence of Electrolyte on Field Orientation

Ryo Sasai, Natsuki Ikuta, and Kiwamu Yamaoka

J. Phys. Chem., **1996**, 100 (43), 17266-17275• DOI: 10.1021/jp961525+ • Publication Date (Web): 24 October 1996

Reversing-Pulse Electric Birefringence of Montmorillonite Particles Suspended in Aqueous Media.† Instrumentation and the Effect of Particle Concentration, Ionic Strength, and Valence of Electrolyte on Field Orientation

Ryo Sasai,‡ Natsuki Ikuta,§ and Kiwamu Yamaoka*,‡

Department of Materials Science, Faculty of Science, Hiroshima University, Kagamiyama 1-3-1, Higashi-Hiroshima 739, Japan, and Applied Physics and Chemistry, Faculty of Engineering, Hiroshima University, Kagamiyama 1, Higashi-Hiroshima 739, Japan

Received: May 24, 1996; In Final Form: August 13, 1996⊗

The electrooptical property of clay particles dispersed in aqueous media was studied with a newly constructed reversing-pulse generator, in which a field-effect transistor (abbreviated as MOS-FET) rather than a vacuum tube was used as the switching element. This pulse generator has the following characteristics: (1) a stable output voltage in the 5−300 V range, (2) a widely variable output pulse duration in the 10 μs−1.2 s range, and (3) a very short time constant of electric pulse (generally 150 ns for buildup and reverse and 50 ns for decay). Moreover, this generator could deliver a single rectangular pulse and/or a reversing pulse to high ionic strength samples, e.g., 0.2 mol dm^{-3} NaCl or $MgCl_2$, because of a high electric current resistance of MOS-FET. By using this new reversing-pulse generator, a study was carried out on the effect of the ionic strength, valence of electrolyte, and particle concentration on the electrooptical and hydrodynamic properties of montmorillonite particles dispersed in aqueous media. The analysis of measured reversing-pulse electric birefringence signals of Na-montmorillonite showed that the particle possesses no *permanent dipole moment* but that an *ion polarization* makes a large contribution to the field orientation. The sodium ion, trapped on the cation-exchangeable site, may be responsible for this *ion polarization*; the Na-montmorillonite particles also form aggregates of *card house structure* at increased concentrations of added sodium ions. In contrast to the Na-montmorillonite particle, reversing-pulse electric birefringence signals of Mg-montmorillonite suspensions showed longer average rotational relaxation times. The signals could not be analyzed theoretically because of larger aggregates of *book house structure*. The optical anisotropy of the clay particle was increased with an increase in Mg^{2+} concentration.

Introduction

To understand the electrooptical phenomena of the surface on disklike colloidal particles in aqueous media, studies on model materials are important. The electrooptical methods are useful to clarify the electric, optical, and hydrodynamic properties of such particles.[1−21] For example, electric birefringence, electric dichroism, and electric light scattering are well-known. In these methods, an electric field is applied to a sample solution for alignment of dispersed particles to the direction of field mostly in a single rectangular pulse. If a reversing pulse (rectangular electric pulses with consecutive positive and negative polarities) is applied to a sample solution, the responding signal yields more useful information on the electric properties of dispersed particles, unobtainable by other physicochemical techniques. These methods have been already applied to clay particles,[3,7,8,18,22−25] biopolymers, such as nucleic acids and proteins,[4,12,13,26−35] and other polyelectrolytes[33,36−43] with many valuable results.

In these electrooptical measurements, an ideal electric field pulse should satisfy the following conditions: (1) the production of a wide and continuously variable pulse voltage, (2) the short time constants for an output electric field pulse at buildup, reverse, and decay, (3) the continuously variable pulse duration over a wide time scale, (4) the application of an electric field pulse to high-conductivity samples, and (5) the easy generation of a reversing-electric pulse form. The electrooptical measurement is often performed on an apparatus which fulfills only some of the above-mentioned conditions. The switching of electric pulses is usually achieved by vacuum tubes in a reversing-pulse generator.[21] This apparatus is quite effective for the output of the high-voltage electric pulse but practically ineffective for the low-output voltage electric pulse.

A well-defined short-width field pulse is difficult to produce with a vacuum-tube pulse generator. The transient signal from a sample solution with particles of small hydrodynamic size is always influenced by the instrumental time constant of comparable magnitudes. Moreover, the pulse field results in sagging, when a long-width field pulse is applied; this is a severe drawback for measuring the large-size particles. The single-square wave line-pulse generator[44] can deliver a field pulse with a short time constant to the sample, suitable for the high-field short-duration pulse, and can be applied to a high-conductivity sample. The line pulser as well as vacuum-tube pulsers are, however, not convenient for the long-duration reversing pulse for the measurement of large particles such as clays and biocolloids, because an extremely low-field strength and the long-width field pulse must be employed to measure the transient electrooptical effect, which is often saturated in the low field region ($\leq$1 kV cm^{-1}).[8,18,22,25] Therefore, a new reversing-pulse generator should be designed to produce for

† Electrooptics in Dispersed Systems Series. 5. Part 4 of this series is given in ref 22.
‡ Department of Materials Science.
§ Applied Physics and Chemistry.
* To whom correspondence should be addressed.
⊗ Abstract published in *Advance ACS Abstracts,* October 1, 1996.

S0022-3654(96)01525-0 CCC: $12.00

measuring large-size particles in aqueous media. The description of the present apparatus with a MOS-FET reversing pulse generator will be given in the Instrumentational Section.

The electrooptical study of montmorillonite particles in aqueous media was initiated by O'Konski and Zimm with a dc electric field.[3] They observed a sign reversal of steady-state electric birefringence from negative to positive with increasing field strengths.[3,8,18,23,24] Subsequently, Shah et al. have explained this phenomenon by assuming the out-of-plane transverse *permanent dipole moment* in the disklike particle.[8] From electric birefringence measurements with samples at various concentrations and diameters of particles, Yoshida et al., however, suggested that the particle possessed no such transverse *permanent dipole moment*.[18] Using a new reversing-pulse generator, we have also studied the electrooptical properties of montmorillonite dispersed in aqueous media by the reversing-pulse electric birefringence method (hereafter abbreviated RPEB).[22,24,25] These results indicated that montmorillonite particle has no *permanent dipole moment*, and that the ion-induced dipole moment, which is slowly induced with applied field and saturated at a certain field strength, was responsible for the anomalous sign-reversal, i.e., the phenomenon that the sign of the steady-state electric birefringence reverses from negative to positive.[22,24,25] On the basis of these results,[22,24,25] we suggested that the field orientation of montmorillonite particle results from the following mechanism. At extremely low fields (steady-state electric birefringence is negative), the symmetric axis of the particle is parallel to the direction of an applied electric field, but this symmetric axis turns to be perpendicular to the field direction at moderately high fields (steady-state electric birefringence is positive). In this paper, quantitative studies will be presented on the effect of the concentration of montmorillonite particles and the ionic strength and valence of added electrolyte on the field orientation by the new RPEB apparatus.

Instrumentational Section

Reversing-Pulse Electric Birefringence Apparatus. An RPEB instrument consists of an optical system and a newly constructed reversing-pulse generator (hereafter abbreviated as RPG).

Optical System. Figure 1a shows the block diagram of RPEB instrument. An NEC GLG5350 5 mW He−Ne gas laser is used as the light source. The polarization plane of the incident light beam is oriented at 45° relative to the direction of the applied electric field by a polarizer. The elliptically polarized light generated by a sample solution passes through a quartz quarter-wave plate and an analyzer, to a Hamamatsu R1398 head-on type photomultiplier. The photoelectric current is amplified by an operation amplifier and detected with a digital TCDE-4000 two-channel wave memory (Riken Denshi Co., Tokyo). The signals are accumulated and stored in a microcomputer. Kerr cells with electrodes made of stainless steel are a cylindrical and demountable type.[21] The optical path length is 4 cm and the electrode gap is 0.443 cm to detect a weak signal at extremely low fields. The detailed description of the optical system is given elsewhere.[21]

Reversing-Pulse Generator. Figure 1b shows the block diagram of a newly constructed RPG. A pulse generator (hereafter abbreviated as PG), whose pulse duration is variable from 10 μs to 1.2 s, generates an output single rectangular-voltage pulse (+5 V), which is then fed to a driver amplifier (hereafter abbreviated as DA) circuit. This DA circuit reshapes the voltage pulse to shorten the time constants of buildup and decay for driving the final discharge unit (hereafter abbreviated as DU). A Hitachi 2SK534 field effect transistor (hereafter abbreviated as MOS-FET: maximum endurable voltage 800 V and electric-current 5 A) in DU is driven by an output single rectangular pulse from DA. The DU generates a high-voltage single square pulse at the same voltage, as supplied from the dc stationary-voltage power supply (hereafter abbreviated as HV). This new RPG can generate not only a single rectangular-voltage pulse but also a reversing-voltage pulse, with an instantaneous polarity reversal. In generating the reversing pulse, the PG generates two independent single rectangular voltage pulses of the same polarity, the second output single-square voltage pulse fed to DA(−) is delayed exactly by the pulse duration of the first and generated. This two voltage pulses are fed to the DA(+) and DA(−) and are transformed to voltage pulses with different polarities in the DU(+) and DU-(−). The output voltage pulses with different polarities are combined at a load resistor (R_L) to deliver a reversing voltage pulse to the Kerr cell.

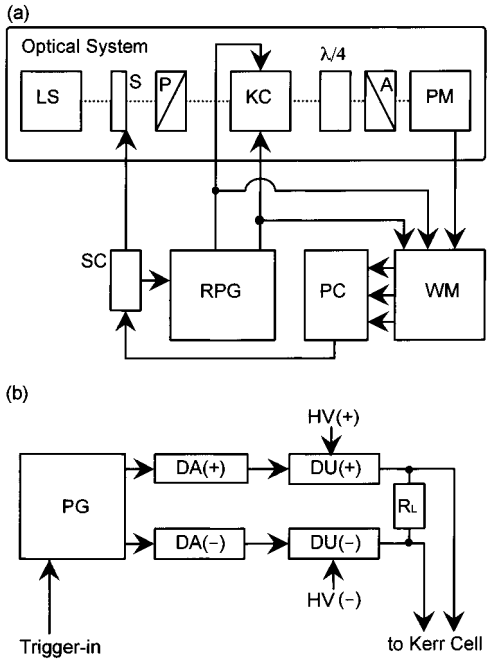

Figure 1. Schematic diagram of reversing-pulse electric birefringence apparatus (a) and new reversing-pulse generator (b). (a) LS, light source (He−Ne laser); S, shutter; SC, shutter controller; P, Glan-Taylor polarizer; KC, Kerr cell; $\lambda/4$, quartz quarter-wave plate; A, Glan-Thompson analyzer; PM, head-on photomultiplier; WM, two-channel transient wave memory; PC, 16-bit microcomputer with display; RPG, new reversing-pulse generator. (b) PG, pulse generator; DA, driver amplifier; DU, discharge unit; R_L, load resistor. (+) and (−) indicate the circuits for producing either positive or negative voltage pulse. (+) is used for producing a single square-wave voltage pulse.

Figure 2a shows the detailed circuitry of DA. An input voltage pulse (+5 V) is electrically isolated from PG by element B, a photocoupler (HP 6N137), to shut out electric noise from PG entering the DA unit for stable high-speed response. The rectangular voltage pulse is amplified and reshaped, and the rectangular output pulse with a magnitude higher than +10 or −10 V is produced for driving DU. Figure 2b shows the detailed circuitry of DU. The HV always supplies the high voltage to the *drain* (D of Figure 2b) of MOS-FET. When a driver pulse from DA is fed to the *gate* (G of Figure 2b) of MOS-FET, the rectangular pulse, which had the same voltage as that of HV, supplies to R_L from the *source* (S of Figure 2b) of MOS-FET.

Characterizations between this new RPG and our previous RPG with vacuum tubes as the switching element are compared

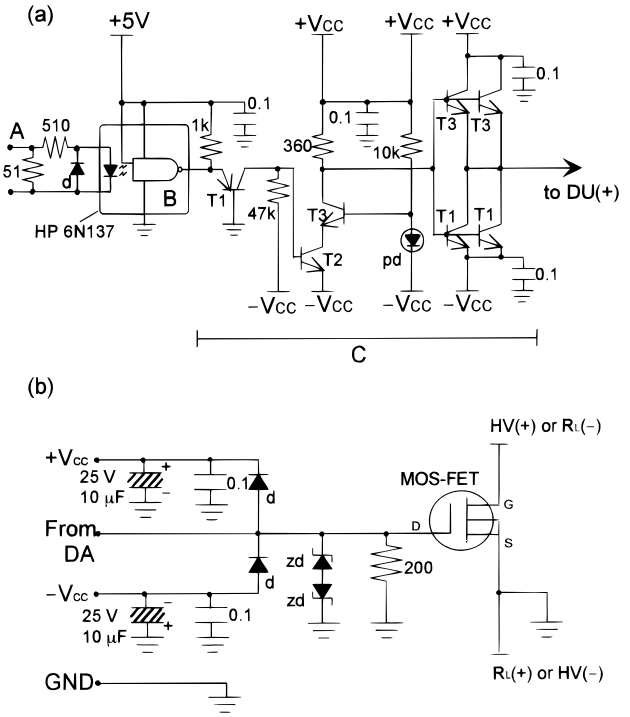

Figure 2. (a) Driver amplifier circuit and (b) discharge unit. Circuit (a) delivers a single voltage pulse for driving a Hitachi 2SK534 field effect transistor (MOS-FET) of the discharge unit. Element B photocoupler HP 6N137 separates circuit A from the remaining circuit C electrically. Two identical units are needed for generating a reversing pulse of opposite polarities. In (b), MOS-FET is used as a switching element. When a single square-wave pulse is produced from this pulse generator, the (+) unit is used (HV(+)−R_L(+) in combination). When the reversing pulse is produced from this pulse generator, two discharge units must be used simultaneously (HV(+)-R_L(+) and HV(−)−R_L(−) in combinations). A Kerr cell is connected parallel to R_L. HV: the high-voltage direct-current power supply. d, diode; pd, photodiode; T, transistor (T1, SA1160; T2, SC1815; T3, SC2500); zd, Zener diode. The resistance is in Ω, unless otherwise stated. The capacity is in microfarads, unless otherwise stated.

TABLE 1: Comparison between New and Old Reversing-Pulse Generators

	pulse shape	applied voltage	pulse duration	time constants t_B[b]/ s	t_R[c]/ s	t_D[d]/ s	*Is*[a]
new	single-square	5−300 V	10 μs−1 s	150		50	0−0.2
	reversing	5−200 V	10 μs−1 s	150	150	50	0−0.2
old[e]	single-square	300 V−6 kV	10 μs−10 ms	400		600	0−0.01
	reversing	300 V−6 kV	10 μs−10 ms	400	800	600	0−0.01

[a] Ionic strength. [b−d] The time constants of the buildup, reverse, and decay part, respectively. [e] Details of the old reversing-pulse generator are described in ref 21.

in Table 1. The time constants of the new RPG are reduced to about $^1/_3$−$^1/_{10}$ of those of the previous one, because the responses of the DA circuit and DU unit with MOS-FET as the switching element are improved. This new RPG may be utilized to evaluate the electrooptical and hydrodynamic parameters and the structure of smaller macromolecules, for instance, short DNA, protein, and the protein−nucleic acid complexes in ionic solution, because of the stable electric pulse with short time constants. However, it can apply only low-field strength pulse (up to ca. $^1/_7$ of the previous one) to a sample solution, because of the low voltage tolerance of the present MOS-FET, but can possibly deliver a field pulse width variable up to 1.2 s. This maximum pulse duration is 400 times long, as compared with the previous one; therefore, the new RPG can also be utilized for larger colloidal particles, e.g., clay and bacteria. The DU circuitry with MOS-FET can deliver a stable electric pulse to a sample solution with high conductivity (up to 0.2 mol dm^{-3} NaCl and/or $MgCl_2$) or under the physiological condition, i.e., in 0.15 mol dm^{-3} NaCl solution. With such a long pulse applied to a high-conductivity sample, however, the temperature jump probably occurs unavoidably due to Joule heat. When a reversing pulse is applied, it is possible to deliberately change a pulse duration as well as a field strength of the first relative to the second pulse, because each circuitry can independently generate these two pulses.

Experimental Section

Preparation of Montmorillonite Suspensions. A montmorillonite sample (K10), purchased from Aldrich Chemical Co., was used. The suspension of montmorillonite was prepared in the following steps. (1) The K10 sample was added to double-distilled water under stir and the suspension was stirred for 2 days. (2) To convert the counterion to sodium ions, the solvent was first replaced with 0.3 mol dm^{-3} NaCl, by adding a high-concentration NaCl solution to sample (1) under stir, and the suspension was stirred for an additional day. (3) To dissociate and disperse aggregated particles, the suspension was sonicated at 0 °C at a power level of 200 W (20 kHz) for 20 min. (4) To remove the remaining metal ions, ethylenediaminetetraacetic acid disodium salt (Na_2EDTA) was added to the suspension, which was then dialyzed against 0.3 mol dm^{-3} NaCl for 1 day to remove excess Na_2EDTA. (5) To make the suspension salt-free, dialysis against the double-distilled water (8 dm^3) was continued for 4 days. (6) To dissociate and disperse particles reaggregated in the course of the dialysis against 0.3 mol dm^{-3} NaCl, sample (5) was sonicated under the same condition as (3). (7) To remove the remaining aggregated or large-size particles, centrifugation was performed at 3000 rpm for 20 min. The supernatant was collected and used as the stock suspension. This supernatant was then stored at room temperature.

The concentration of stock suspension was estimated to be 0.29 g dm^{-3}, by measuring the weight of the anhydrous sample prepared by the freeze-drying and subsequently heat-drying method in vacuo. For RPEB measurements, the stock suspension was diluted with double-distilled water (the concentration dependence) and with NaCl solution (the ionic-strength dependence). Na^+ counterions were replaced to Mg^{2+} ions by dialyzing the stock Na-montmorillonite suspension first against 0.1 mol dm^{-3} $MgCl_2$ solution for a day, and then against the double-distilled water (8 dm^3) for 4 days. This dialyzed suspension was used as the salt-free Mg-montmorillonite suspension, to which $MgCl_2$ solution was added to prepare samples at various ionic strengths.

Electron Microscopic Photograph of Montmorillonite Particles. Figure 3b shows an electron-microscopic photograph of Na-montmorillonite particles. From this photograph, the average diameter of Na-montmorillonite particles was estimated to be ca. 275 nm. Particles are not a truly circular disk but rather fractal, showing no specific shape, and also are not monodisperse but polydisperse in size in the dried suspension.

Analytical Section

The experimental data were analyzed as below, and the results from these analyses are presented in the Results and Discussion.

RPEB Transient Signal at Low Field. RPEB transient signals at low fields, i.e., the Kerr law region, were analyzed by the curve-fitting method, with the RPEB transient theory, derived by Yamaoka et al. on the basis of *ion-fluctuation* (hereafter abbreviated as the YTS theory).[25] The theory, applicable only in the Kerr-law region, is based on the concept

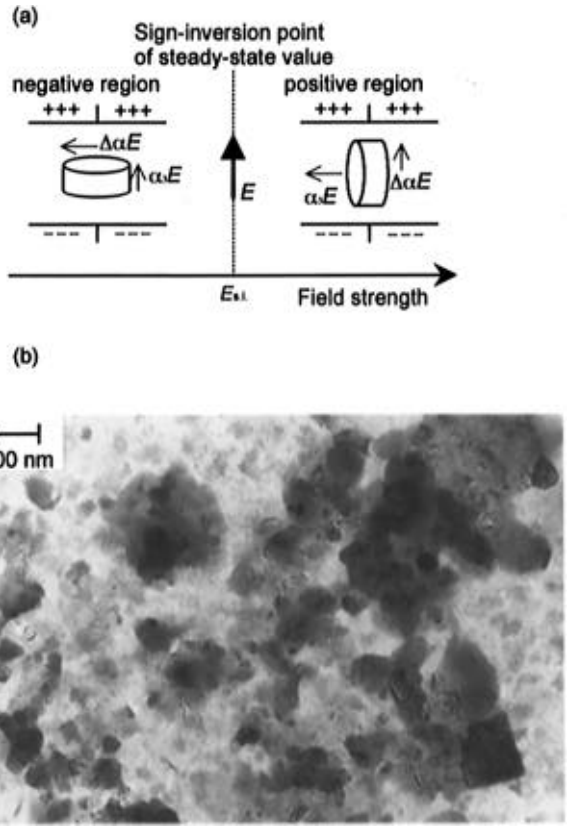

Figure 3. Schematic presentation of particle orientation against field strength (a) and electron microscopic photograph of Na-montmorillonite dispersed particles (b). Particle concentration: 0.005 g dm^{-3}. Below the sign-inversion field $E_{s.i.}$, the plane of the particle is oriented perpendicular to the direction of electric field (left). Above $E_{s.i.}$, the plane of the particle is oriented parallel to the direction of electric field (right).

that the orientation of solute molecules results from an instantaneously induced electric dipole moment ($\Delta\alpha' E$) and an electric dipole moment ($\alpha_3 E$) induced by the ion-atmosphere fluctuation with a finite relaxation time (τ_I). This theory is expressed as[25]

$$\Delta_B(t) = \frac{\Delta n_B(t)}{\Delta n_B(\infty)} = 1 - \left[1 + \left(\frac{6\Theta\tau_I}{1-4\Theta\tau_I}\right)\left(\frac{q}{q+1}\right)\right]e^{-6\Theta t} + \left(\frac{6\Theta\tau_I}{1-4\Theta\tau_I}\right)\left(\frac{q}{q+1}\right)e^{-(2\Theta+\tau_I^{-1})t} \quad (1)$$

$$\Delta_R(t) = \frac{\Delta n_R(t)}{\Delta n_R(0)} = 1 - \left(\frac{6\Theta\tau_I}{1-4\Theta\tau_I}\right)\left(\frac{2q}{q+1}\right)[e^{-6\Theta t} - e^{-(2\Theta+\tau_I^{-1})t}] \quad (2)$$

$$\Delta_D(t) = \frac{\Delta n_D(t)}{\Delta n_D(0)} = e^{-6\Theta t} \quad (3)$$

where Θ is the rotational diffusion coefficient, τ_I is the relaxation time of the ion-atmosphere fluctuation, q ($=\alpha_3/\Delta\alpha'$) is the ratio of the polarizability due to ion atmosphere fluctuation, α_3, and the polarizability, $\Delta\alpha'$, responsible for an instantaneously induced electric dipole moment (all other notations should be refined to ref 25). The curve fitting by the classical Tinoco and Yamaoka theory (hereafter abbreviated as the TY theory),[45] which considers the orientation due to the permanent dipole (μ) and instantaneously induced ($\Delta\alpha' E$) dipole moments, was also carried out. The TY theory is given as

$$\Delta_B(t) = 1 - \frac{3}{2}\left(\frac{Q}{Q+1}\right)e^{-2\Theta t} + \frac{1}{2}\left(\frac{Q-2}{Q+1}\right)e^{-6\Theta t} \quad (4)$$

$$\Delta_R(t) = 1 - \left(\frac{3Q}{Q+1}\right)(e^{-2\Theta t} - e^{-6\Theta t}) \quad (5)$$

$$\Delta_D(t) = e^{-6\Theta t} \quad (6)$$

where Q ($=\mu^2/kT\Delta\alpha'$) is the ratio of the permanent dipole and instantaneously induced dipole moments, k is the Boltzmann coefficient, T is the absolute temperature.

Field-Strength Dependence of Steady-State Electric Birefringence. The field-strength dependence of steady-state electric birefringence was analyzed by the curve-fitting method with the PD-SUSID orientation function, derived in part 4 of this series,[22] for the disklike particle, which possesses three electric moments, i.e., the permanent dipole (μ) transverse to the disk plane and the unsaturable ($\Delta\alpha' E$) and saturable ($\Delta\sigma E$) induced dipole moments, where $\Delta\sigma$ is the polarizability, responsible for an ion polarization. The limiting specific phase retardation per path length, d, at infinitely high electric fields, $(\delta_{st}/cd)_\infty$, where c is the mass concentration, and the corresponding intrinsic quantity, $(\delta_{st}/cd)_{intr}$, are related as

$$\left(\frac{\delta}{cd}\right)_\infty = \left(\frac{\delta}{cd}\right)_{intr} \cdot \Phi \; (E \rightarrow \infty) \quad (7)$$

where $\Phi(E\rightarrow\infty)$ is the orientation function at infinitely high fields, being equal to unity for rigid particle but equal to $-1/2$ for disklike particle.[46] The electrical and optical properties of montmorillonite particles were estimated quantitatively.

Field-off Decay Signal. The field-off electric birefringence decay signal yields information on the hydrodynamic size of dispersed particle. When a sample is monodisperse, the decay signal is usually expressed with a single-exponential curve. The decay signal of a polydisperse system, however, cannot be expressed with such a curve because of the distribution of size, length, and so on. When the distribution is considered, the decay signal is given as[1]

$$\Delta n(t) = \sum_i \Delta n_{st,i} e^{-t/\tau_i} \quad (8)$$

where τ_i is the rotational relaxation time of the ith component, $\Delta n_{st,i}$ is the electric birefringence of the ith component at $t = 0$, i.e., the steady-state electric birefringence.

The decay signal is analyzed according to two methods: (1) the peeling method, which presumes that the signal is the sum of single-exponential curves,[1] and (2) the area method, in which the area surrounded between the measured decay curve and the baseline yields the birefringence-average relaxation time, $\langle\tau\rangle_{EB}$.[52] According to (1), the relaxation time $\langle\tau\rangle_{EB}$ was defined as

$$\langle\tau\rangle_{EB} = \sum_i a_i\tau_i \qquad \sum_i a_i = 1 \quad (9)$$

where a_i is the relaxation intensity of the ith component. In the case of (2), $\langle\tau\rangle_{EB}$ is given as

$$\langle\tau\rangle_{EB} = \int_0^\infty \frac{\Delta n(t)}{\Delta n_{st,i}}\,dt \quad (10)$$

Values of $\langle\tau\rangle_{EB}$, obtained by either methods for the sample with a size distribution, show the field-strength dependence because of the different orientation degree of each component at a given field strength. To estimate the rotational relaxation time at complete orientation, the measured $\langle\tau\rangle_{EB}$ values are extrapolated

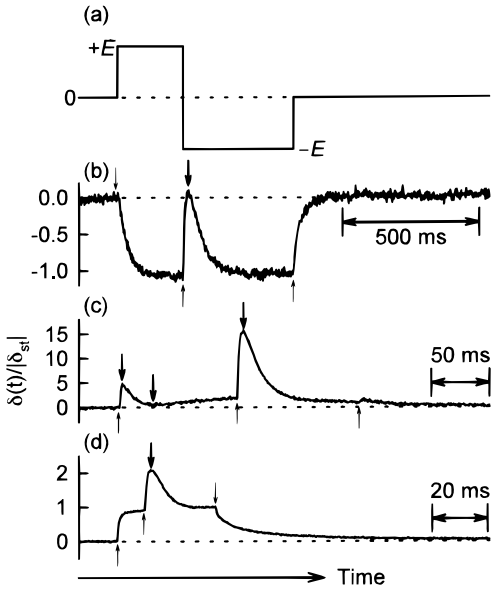

Figure 4. RPEB signals of Na-montmorillonite suspension normalized by the absolute magnitude of steady-state phase retardation $|\delta_{st}|$. A schematic reversing-pulse pattern (a). RPEB signals without added sodium ion at $c = 0.029$ g dm^{-3} (b−d): (b) $E = 22$ V cm^{-1} and $\delta_{st}/cd = -0.42$ deg dm^3 g^{-1} cm^{-1}; (c) $E = 91$ V cm^{-1} and $\delta_{st}/cd = 0.12$ deg dm^3 g^{-1} cm^{-1}; (d) $E = 179$ V cm^{-1} and $\delta_{st}/cd = 2.89$ deg dm^3 g^{-1} cm^{-1}. Thick arrows indicate the positions of maximum and minimum. Thin arrows show the field-on, reverse, and field-off points of applied electric pulses. Note the change of time scale of signals in parts.

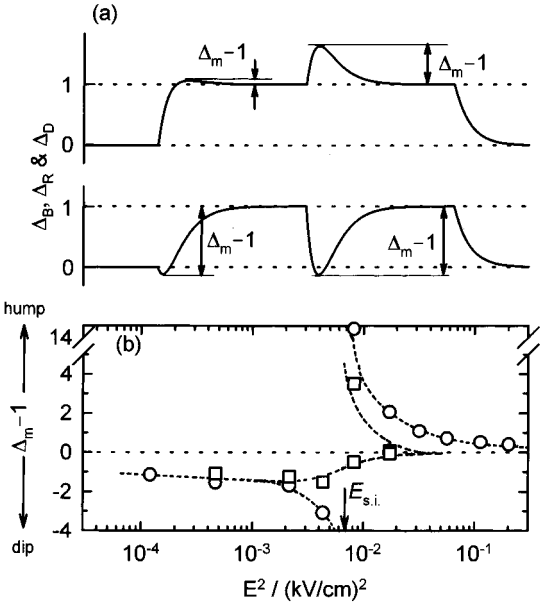

Figure 5. Schematic presentation of normalized RPEB signals, Δ_B, Δ_R, and Δ_D, with humps (upper) and dips (lower) (a) and experimentally observed height of humps and depth of dips, $\Delta_m - 1$, for Na-montmorillonite suspension (c, 0.029 g dm^{-3} and nearly no added salt, $Is \approx 0$) (b). (○) buildup process; (□) reverse process. The arrow shows the inversion field strength $E_{s.i.}$.

to infinitely high fields. The relaxation time obtained from such an extrapolation reduces to the weight-average rotational relaxation time τ_w. The weight-average diameter $\langle d \rangle_w$ of a very thin oblate ellipsoid particle may be evaluated from τ_w as[47]

$$\langle d \rangle_w = [9kT\tau_w/2\pi\eta_0]^{1/3} \qquad (11)$$

where η_0 is the viscosity of solvent, k is the Boltzmann coefficient, and T is the absolute temperature.

Results and Discussion

Na-Montmorillonite Suspensions. In this section, descriptions are given of the effect of the particle concentration and the ionic strength of the sodium ion on the electrooptical and hydrodynamic properties of Na-montmorillonite particles.

Reversing Transient Signals. In Figure 4, typical RPEB transient signals of Na-montmorillonite suspension ($c = 0.029$ g dm^{-3} and $Is = 0$) are illustrated. Signals of the *negative* sign with deep dip (thick arrow) appear at low fields (Figure 4b). With an increase in field strength, however, anomalous RPEB signals (Figure 4c) become predominant in the vicinity of the field strength of the sign inversion, $E_{s.i.}$, where the sign of the steady-state electric birefringence is reversed.[22] This signal shows both dip and hump at the buildup and reverse portions. At field strengths higher than $E_{s.i.}$, RPEB signals of the *positive* sign with the humps in reverse process (thick arrow) appear after the sign inversion of the steady-state electric birefringence (Figure 4d). The pattern of a hump (maximum) and a dip (minimum), $\Delta_m - 1$, is illustrated in Figure 5, where Δ_m is either a maximum or minimum value of an RPEB signal normalized by the steady-state value. Values of $\Delta_m - 1$, calculated from the measured signals, are plotted against the second power of the field strength in Figure 5b. At $E \leq E_{s.i.}$ ($E_{s.i.} = 68.3$ V cm^{-1}), RPEB signals show a dip in reverse at extremely low fields, and a dip in buildup with the increase in field strength (Figure 4b). These dips become deeper with increasing field strength, and the depth reaches a maximum ($\Delta_m - 1 = -3$) at $E_{s.i.}$. In the vicinity of $E_{s.i.}$, RPEB signals show both dip and hump in the buildup and reverse processes (Figure 4c). This observation may be attributed to the different degree of field orientation of particle in the suspension; the present sample is polydisperse and hence the orientation axes of disklike particles of various sizes are mixed near $E_{s.i.}$ as indicated in Figure 3a. In the reverse and/or buildup processes at $E \geq E_{s.i.}$, humps are noted, the height which are maximal ($\Delta_m - 1 = 14$) near $E_{s.i.}$. The hump monotonically decreases with further increasing field strength, disappearing at higher field strengths. This disappearance of hump is probably due to the fact that the instantaneously induced dipole moment proportional to the field strength becomes predominant in field orientation. Similar phenomena are observed at higher concentrations of particles and added sodium ions.

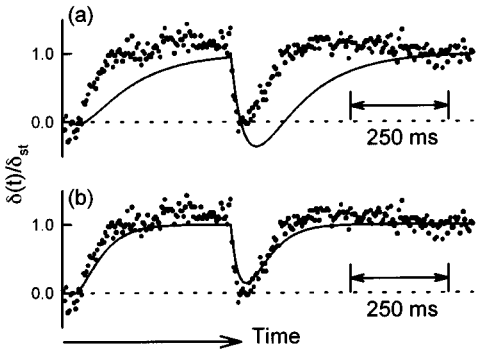

Figure 6. Measured and simulated RPEB signals of Na-montmorillonite suspension. Dots: measured signal (b) in Figure 4. The sampling time between two successive points in observed signal is 0.4 ms. Solid lines: simulated signals. Parameters for simulated curves: $\langle \tau \rangle_{EB} = 39.8$ ms and $Q = -6.7$ from the Tinoco−Yamaoka theory in (a) and $\langle \tau \rangle_{EB} = 39.8$ ms, $\tau_1 = 59.7$ ms, and $q = -6.7$ from the Yamaoka−Tanigawa−Sasai theory (eqs 1−3) in (b).

Figure 6 shows the analysis of a RPEB signal of the Na-montmorillonite suspension ($c = 0.029$ gdm^{-3}, $Is = 0$, $E = 11$ Vcm^{-1}) with two RPEB theories.[24,45] The solid line in Figure 6a is the theoretical curve calculated from the TY theory (eqs

TABLE 2: Electrical and Hydrodynamic Properties of Na-Montmorillonite Particles in Aqueous Media Estimated from RPEB Signals

c/g dm^{-3}	Is	q^a	τ^{*b}
0.005	0		
0.010	0	−6.7	1.4
0.029	0	−6.7	1.5
0.058	0	−5.0	1.9
0.145	0	−6.7	1.3
0.029	0.0001	−5.0	0.89
0.029	0.0005	−2.9	0.60

[a] q equals $\alpha_3/\Delta\alpha'$. [b] τ^* equals to τ_l/τ_θ ($\tau_\theta = {}^1/_6\theta$).

4−6), by assuming the presence of the permanent dipole (μ) and induced dipole ($\Delta\alpha$) moments with a ratio ($Q \equiv \mu^2/\Delta\alpha kT$ of −6.7).[45] This theoretical curve could reproduce no measured RPEB signals at any particle and added sodium ion concentrations. Thus, this result should be taken as the evidence that the Na-montmorillonite particle possesses no *permanent dipole moment*. The solid line in Figure 6b is the theoretical curve calculated with eqs 1−3; it is in good agreement with all measured RPEB signals of the Na-montmorillonite suspension under the present condition. These results lead to the conclusion that the orientation of the Na-montmorillonite particle is due to the electric moment induced by *ion polarization* within the finite time after an application of electric pulse field.

The electrical and hydrodynamic parameters evaluated by curve fitting with the YTS theory are given in Table 2. The polarizability ratio, q, and the reduced relaxation time $\tau^* = \tau_l/\tau_\theta$ ($\tau_\theta = {}^1/_6\Theta$), are nearly constant with particle concentration but decreased with increasing concentrations of added sodium ions. This result reflects that sodium ions trapped in cation-exchangeable sites become immobilized with the increase in ionic strengths, probably because of the predominant adsorption of the sodium ions onto the site. The result also supports the notion that the fluctuation of the trapped sodium ions on cation-exchangeable sites is responsible for the ion-atmosphere polarizability α_3.

Field-Strength Dependence of Steady-State Electric Birefringence. Figure 7 shows the field-strength dependence of the steady-state electric birefringence at various concentrations of particles and added sodium ions. The sign inversion of the steady-state electric birefringence was observed for all Na-montmorillonite samples in the low-field region (cf. inserts of Figure 7). The difference in the field strength dependence of the steady-state electric birefringence of each sample becomes obvious at increased particle concentrations and increased field strengths (Figure 7a); moreover, the normalized quantity δ_{st}/cd at a given field strength decreases with increasing particle concentration. The decrease of the transmissivity of incident light with the increase in particle concentrations is observed; therefore, the origin of this decrease of δ_{st}/cd may be due to the increase in the forward light-scattering intensity at higher particle concentrations. Figure 7b shows the field strength dependence of the steady-state electric birefringence at various ionic strengths of added sodium ions. The field of sign inversion, $E_{s.i.}$, shifts to higher field strengths with increasing ionic strength (insert of Figure 7b). This result indicates that the *ion polarization* is responsible for the sign inversion of the steady-state electric birefringence.

Comparison with RPEB Theoretical Curves. Solid lines in Figure 7 are the best-fitted theoretical PD-SUSID orientation curves calculated for the disklike particle.[22] The experimental field strength dependence of the steady-state electric birefringence was reproduced well with the PD-SUSID function in each case, even if the concentrations of particle and added sodium

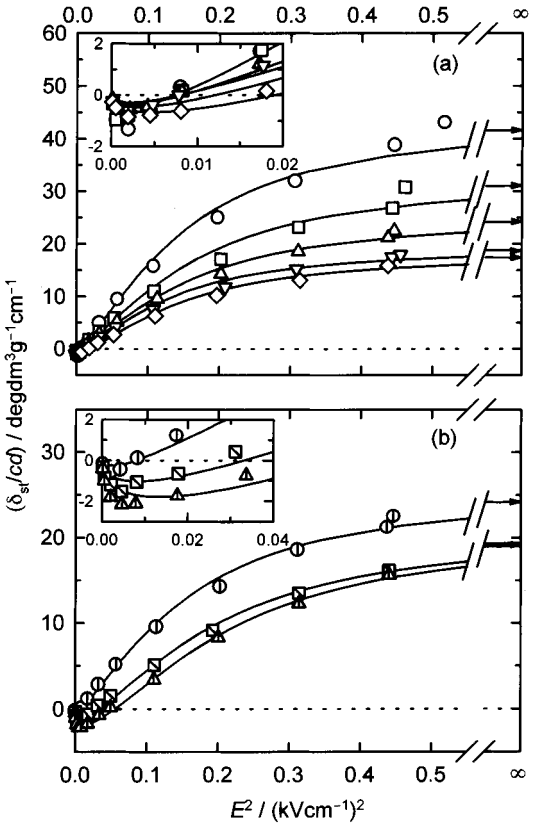

Figure 7. Field-strength dependence of the steady-state electric birefringence of montmorillonite suspensions. The optical phase retardation per path length d of a Kerr cell (4 cm) normalized by the concentration of montmorillonite suspension c, (δ_{st}/cd) in deg dm^3 g^{-1} cm^{-1}, is plotted against the second power of applied electric field strength E^2. Symbols: experimental data. Solid lines: the best-fitted theoretical SUSID orientation functions. (a) Data measured without added sodium ion; c = 0.005 g dm^{-3} (○), 0.010 (□), 0.029 (△), 0.058 (▽), 0.145 (◇). (b) Data measured at various ionic strength Is of added sodium ion at a constant c (=0.029 g dm^{-3}). Is = 0 (○), 0.0001 (□), 0.0005 (△). Inserts in (a) and (b): the abscissa on an expanded scale. Values of δ_{st}/cd at infinite fields are indicated with arrows on the right ordinate.

ions are varied widely. The electrooptical properties of the Na-montmorillonite particle, estimated from these best-fitted theoretical curves, are given in Table 3. The result again indicates that the Na-montmorillonite particle possesses no *permanent dipole moment*; the notion already supported by RPEB data (Figure 6b). This conclusion agrees with the previous reports[22,24,25] and also with a report by Yoshida et al.,[18] in contrast with the results reported by Shah.[8] The polarizability, $\Delta\alpha'$, due to an unsaturable induced dipole moment and the polarizability, $\Delta\sigma$, responsible for an saturable induced dipole moment are constant in the low concentration range (at $c \leq$ 0.029 g dm^{-3}), indicating that no interparticle electrostatic and hydrodynamic interaction exists. However, the reduced saturated steady-state electric birefringence, $(\delta_{st}/cd)_{intr}$, which reflects the optical property, free from electric property, of dispersed particles, is largely changed. This decrease may be due to the increase in the forward light scattering at higher particle concentrations. In $c >$ 0.029 g dm^{-3}, both $\Delta\alpha'$ and $\Delta\sigma$ are increased probably because of the occurrence of the interparticle electrostatic interactions between electric double layers of dispersed particles.

When the ionic strength of added sodium ions is increased, the $\Delta\alpha'$ value remains constant, whereas $\Delta\sigma$ is increased to saturation. This result indicates that $\Delta\sigma$ is associated with *ion polarization*; the saturation of ion-induced dipole moment is

TABLE 3: Electrooptical and Hydrodynamic Properties of Na-Montmorillonite Particles in Aqueous Media Evaluated from Field-Strength Dependence of Steady-State Electric Birefringence and Relaxation Time

c/g dm^{-3}	Is	$\Delta\alpha'/10^{-29}$ F m^2	$\Delta\sigma/10^{-29}$ F m^2	μ/C m	E_0[a]/V cm^{-1}	$E_{s.i.}$[b]/V cm^{-1}	$(\delta_{st}/cd)_{intr}$[c]	τ_w/ms	$\langle d\rangle_w$/nm
0.005	0	−1.86	9.3	0	9.3	65.8	−92.5	4.6	298
0.010	0	−1.69	8.5	0	9.8	69.7	−66.6	5.7	321
0.029	0	−1.75	8.8	0	9.6	68.3	−55.1	4.7	300
0.058	0	−2.33	23.3	0	5.9	83.4	−40.7	4.6	298
0.145	0	−2.22	33.3	0	4.9	104	−38.2	3.8	280
0.029	0.0001	−1.71	34.2	0	4.9	139	−44.0	4.2	290
0.029	0.0005	−1.78	62.4	0	3.9	179	−44.1	5.8	322

[a] At this field strength, the saturable induced dipole moment is saturated. [b] This value is the field strength for the sign-inversion point. [c] Values are given by $(\delta_{st}/cd)_\infty \times (-2)$ in deg dm^3 g^{-1} cm^{-1}, where d is the optical path length. $(\delta_{st}/cd)_\infty$ is the limiting value of δ_{st}/cd at infinitely high fields.

probably due to the predominant adsorption of added sodium ions onto cation-exchangeable sites. Since $\Delta\sigma$ values are larger than those of $\Delta\alpha'$, a large electric dipole moment transverse to the disk plane should be induced. The critical field strength, E_0, where the saturable induced dipole moment is saturated, is extremely low (cf. Table 3). This result leads to the conclusion that Na ions adsorbed onto cation-exchangeable sites are responsible for the saturable induced dipole moment, $\Delta\sigma E$, and this dipole moment can easily be saturated at extremely low fields (ca. 4−10 V cm^{-1}) because of the immobility of sodium ions on cation-exchangeable site. At low fields ($E \leq E_0$), the plane of disk is oriented perpendicular to the direction of applied external field because of predominant contribution of the saturable induced dipole moment $\Delta\sigma E$ to the field orientation (cf. Figure 3a). At $E \geq E_0$ but $E \leq E_{s.i.}$, the saturable induced dipole moment is saturated, but the plane of disk is still oriented perpendicular to the field direction. Since the unsaturable induced dipole moment $\Delta\alpha' E$ is smaller than the saturable moment $\Delta\sigma E$, the plane of disklike particle changes at $E_{s.i.}$ from the perpendicular to parallel direction of applied field and remains as such at higher field (Figure 3a). The sign inversion point $E_{s.i.}$ becomes higher with increasing sodium ions added to solution (Table 3). This increase of $E_{s.i.}$ with ionic strength corresponds to the increase of the $\Delta\sigma$, indicating that the polarization of sodium ions adsorbed onto the cation-exchangeable sites is responsible for the sign-inversion phenomenon. The saturated steady-state electric birefringence $(\delta_{st}/cd)_{intr}$ is slightly decreased with increasing ionic strengths, which is probably due to formation of aggregates.

Field-Strength Dependence of $\langle\tau\rangle_{EB}$. Figure 8 shows the field-strength dependence of the electric birefringence-average rotational relaxation time $\langle\tau\rangle_{EB}$ of Na-montmorillonite particles. Since $\langle\tau\rangle_{EB}$ values vary with field strengths, the present Na-montmorillonite sample should have the hydrodynamic size distribution; a fact clearly supported by electron microscopic observations (cf. Figure 3b). Values of $\langle\tau\rangle_{EB}$ show an anomalous field dependence near the $E_{s.i.}$, as indicated with arrows in (a1) and (b1). This anomaly is probably due to the change of an orientational axis (cf. Figure 3a), since the symmetry axis of disklike particle changes from the parallel to perpendicular direction of applied electric field at $E_{s.i.}$, as noted in the above section. The hydrodynamic size distribution, however, may also lead to such an anomalous behavior, which is left open to further experimental and theoretical considerations. To estimate the $\langle\tau\rangle_{EB}$ value at infinitely field strength, i.e., the weight-average rotational relaxation time τ_w, observed $\langle\tau\rangle_{EB}$ values are plotted against E^{-2} (Figure 8 (a2) and (b2)). The τ_w value (cf. Table 3) is independent of the particle concentration (ca. 5 ms) but slightly increased with increasing ionic strength. These results lead to the conclusion that the size of Na-montmorillonite particles becomes slightly larger with an increase in added sodium ions.

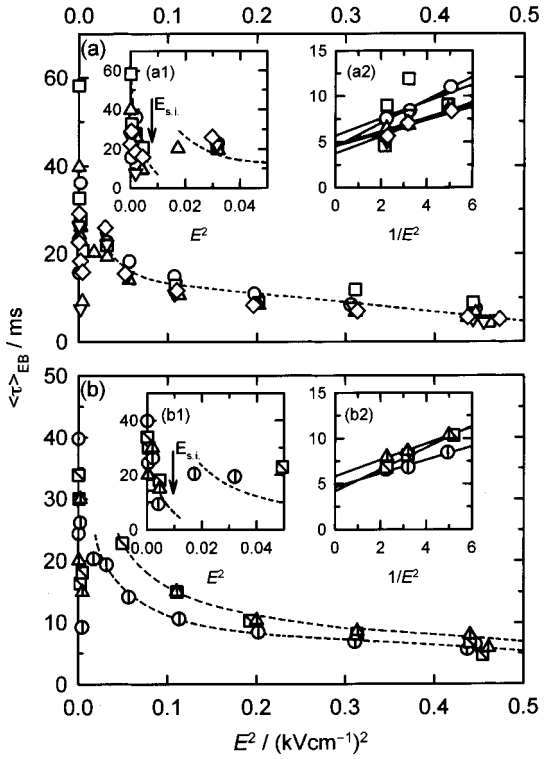

Figure 8. Field-strength dependence of the electric birefringence-average rotational relaxation time $\langle\tau\rangle_{EB}$ evaluated from the decay signal. (a) $\langle\tau\rangle_{EB}$ at various concentrations of Na-montmorillonite particles in the absence of added solution ion. (b) $\langle\tau\rangle_{EB}$ at various ionic strengths at a constant Na-montmorillonite concentration (c = 0.029 g dm^{-3}). Symbols are the experimental data as given in Figure 7. Inserts (a1) and (b1): the expanded abscissa. $E_{s.i.}$: the electric field strength at the sign inversion point. Inserts (a2) and (b2): $\langle\tau\rangle_{EB}$, plotted against $1/E^2$ (in kV^{-2} cm^{-2}) at high fields. Four measured points at high fields are linearly extrapolated to infinitely high fields by the one-dimensional least-squares method (solid lines).

Effect of Particle Concentration and Ionic Strength on the Diameter. Figure 9 shows the dependence of weight-average diameter $\langle d\rangle_w$, calculated from eq 11, of the Na-montmorillonite particle on particle concentration and ionic strength of added sodium ion. The $\langle d\rangle_w$ value is nearly constant at ca. 300 nm regardless of particle concentrations in the absence of added sodium ions. This diameter is very close to that estimated from an electron microscopic observation (ca. 275 nm); therefore, Na-montmorillonite suspensions form neither aggregates nor flocculations in this concentration range. This result supports the notion that the decrease of saturated steady-state electric birefringence is not due to formation of the aggregates at high particle concentrations (vide supra) but due to the forward scattering of light. Since $\langle d\rangle_w$ values are slightly increased (Figure 9b) with increasing ionic strength, aggregates may be formed by added sodium ions. Thus, the decrease in saturated

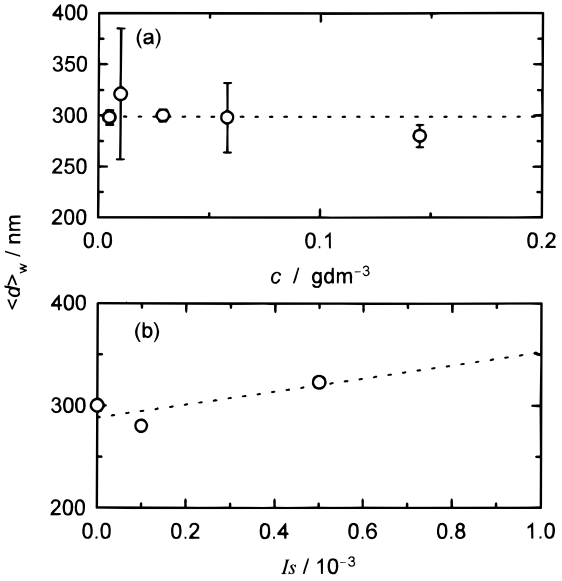

Figure 9. Dependence of the weight-average diameter $\langle d \rangle_w$ of Na-montmorillonite particle on particle concentration and ionic strength. (a) $\langle d \rangle_w$ at various particle concentrations in the absence of added sodium ions. (b) $\langle d \rangle_w$ at various ionic strengths and at a constant particle concentration ($c = 0.029$ g dm^{-3}).

steady-state electric birefringence (cf. Figure 7b) should be associated with a decrease in the optical anisotropy of aggregated particles. The aggregation occurs probably in a random and less ordered fashion; the overall shape of the aggregated particles is said to be in a *card house structure* with many inner cavities.[48,49]

Mg-Montmorillonite Suspension. The birefringence behavior of Mg-montmorillonite suspension is described to ascertain the effect of the valence of counterion.

RPEB Signals. Figure 10 shows RPEB signals of the Mg-montmorillonite, which are quite different from those of Na-montmorillonite. The signals are always positive over the entire range of measured electric field strengths (Figure 10b−g). At $Is = 0$ (Figure 10b−d), the positive signal with a dip appears upon field reversal at extremely low fields (b). With increasing field strength, a hump appears first being followed by a shallow dip (c, d). At $Is = 0.0001$ (Figure 10e−g), the change of a signal profile is ill-defined upon field reversal in the low-field region (e), but a distinct hump appears in the reverse with increasing field strength (f, g). These results indicate that the field orientation of Mg-montmorillonite particle differs from that of the corresponding Na-montmorillonite particle and that the electrical properties are changed by substituting counterions from Na^+ to Mg^{2+}. The Mg-montmorillonite suspension requires a much longer pulse time for reaching the steady-state; hence, the size of Mg-montmorillonite particles should be larger than that of the Na-montmorillonite particles.

Figure 11 shows signal fitting of an observed RPEB pattern of Mg-montmorillonite suspension (cf. Figure 10b) with two different theories. The experimental signal, fitted by the TY theory (upper), which assumes the permanent dipole orientation, or by the YTS theory (lower), which assumes the ionic induced dipole orientation, distinctly differ from these two theoretical RPEB curves. The failure to reproduce the observed RPEB profile should be taken as the strong indication that the orientation mechanism of the Mg-montmorillonite particle is different from the Na-montmorillonite. This difference could result from formation of large aggregations of Mg-montmorillonite particles.

Field-Strength Dependence of Steady-State Electric Birefringence. Figure 12a shows the field strength dependence of the

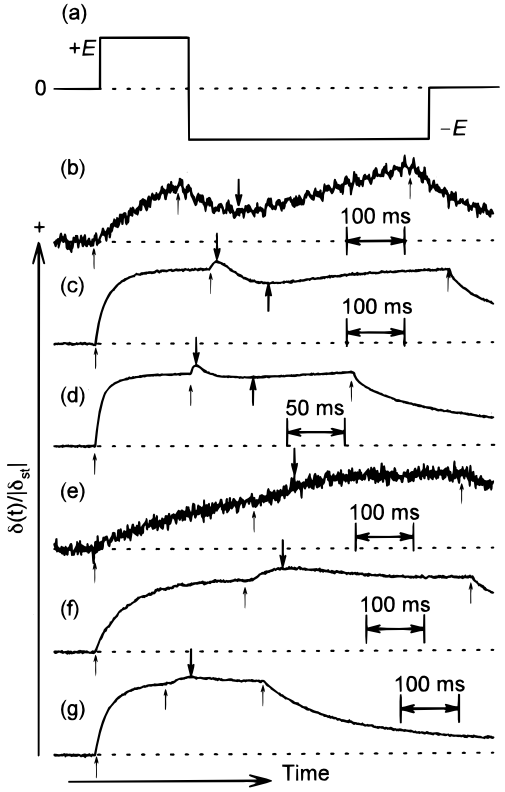

Figure 10. Normalized RPEB signals of Mg-montmorillonite suspensions. (a) Schematic reversing-pulse pattern. (b−d) RPEB signals measured at $c = 0.065$ g dm^{-3} and $Is = 0$; (e−g) $c = 0.065$ g dm^{-3} and $Is = 0.0001$. Applied field strength E in V cm^{-1} and reduced saturated steady-state electric birefringence δ_{st}/cd in deg dm^3 g^{-1} cm^{-1}: 14 and 0.09 (b); 94.6 and 8.63 (c); 238 and 14.1 (d); 13 and 0.48 (e); 102 and 11.7 (f); 236 and 22.2 (g). Thin arrows indicate points of field switching, while thick arrows show either hump or dip. Note the change of time scale of signals in parts.

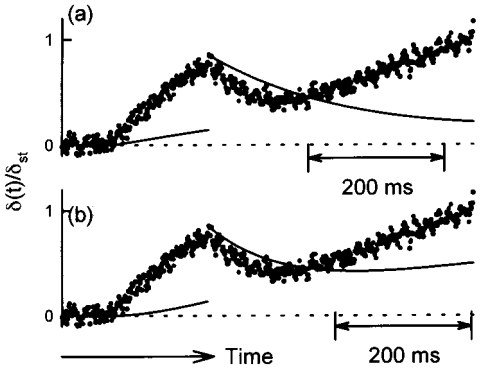

Figure 11. Measured and simulated RPEB signals of a Mg-montmorillonite suspension. Measured signal is (b) in Figure 10. The sampling time between two successive points in observed signal is 0.2 ms. Solid lines are theoretical and drawn with parameters $\langle \tau \rangle_{EB} = 234$ ms and $\beta^2/2\gamma = 3.0$ for the TY theory (a) and $\langle \tau \rangle_{EB} = 234$ ms, $\tau_I = 400$ ms, and $q = 2.0$ for the YTS theory (b).

steady-state electric birefringence of Mg-montmorillonite suspensions, the sign of which is always positive without sign inversion. At higher magnesium ions, the steady-state electric birefringence is higher at a given field strength, two sets of measured field strength dependence (Figure 12a) are superimposed by multiplying by a factor of 1.5. Therefore, with increasing ionic strength, the optical property, but not the electric property, of Mg-montmorillonite is altered. Interestingly, these measured values could not be fitted by any PD-SUSID orientation functions for the disklike particle; therefore, the orientation behavior of Mg-montmorillonite particles cannot be described

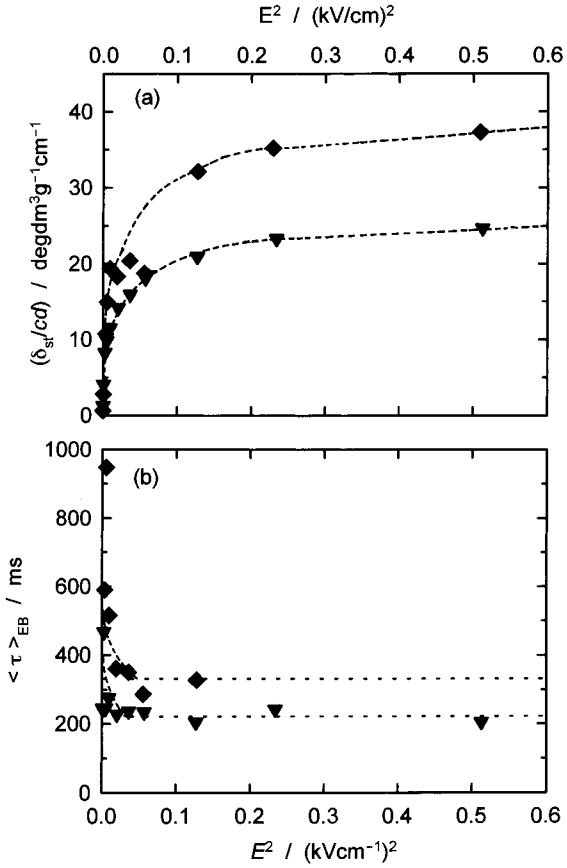

Figure 12. Field-strength dependence of the steady-state electric birefringence (a) and electric birefringence-average rotational relaxation time $\langle\tau\rangle_{EB}$ (b) of Mg-montmorillonite. (▼) $c = 0.065$ g dm^{-3} and $Is = 0$, (◆) $c = 0.065$ g dm^{-3} and $Is = 0.0001$.

TABLE 4: Optical Anisotropy and Diameter of Mg-Montmorillonite in Aqueous Media

c/g dm^{-3}	Is	$(\delta_{st}/cd)_{intr}$[a]/ deg dm^3 g^{-1} cm^{-1}	τ_w/ms	$\langle d\rangle_w$[b]/μm
0.065	0	−51.9	235	1.11
0.065	0.0001	−78.1	322	1.23

[a] This value is given by $(\delta_{st}/cd)_\infty \times (-2)$, where d is the optical path length. $(\delta_{st}/cd)_\infty$ is δ_{st}/cd at infinitely high fields. [b] The diameter of disk obtained from Perrin's equation (eq 7) for an oblate ellipsoid of revolution.

by the simple PD-SUSID orientation mechanism.[22] The formation of aggregates by added magnesium ions could be responsible for the apparently anomalous field orientation of Mg-montmorillonite particles. Table 4 shows the saturated reduced steady-state electric birefringence, $(\delta_{st}/cd)_{intr}$, evaluated from the data measured at high fields where a gradual leveling-off is apparent. Values of $(\delta_{st}/cd)_{intr}$ are higher at higher ionic strength of magnesium ions, indicating that the optical anisotropy of the Mg-montmorillonite particle increases with increasing ionic strength of the magnesium ions.

Field-Strength Dependence of $\langle\tau\rangle_{EB}$. Figure 12b shows the field-strength dependence of $\langle\tau\rangle_{EB}$. Values of $\langle\tau\rangle_{EB}$ are markedly larger for the Mg-montmorillonite particle than for Na-montmorillonite, indicating that the Mg-montmorillonite particles no doubt form large aggregates, which grow with an increase in ionic strength. The average diameter $\langle d\rangle_w$ of Mg-montmorillonite particles (ca. 1.2 μm), evaluated from the measured $\langle\tau\rangle_{EB}$ data and given in Table 4, is about 4 times as large as that of the nonaggregated Na-montmorillonite particle (ca. 300 nm). Judged from the optical anisotropy factor of Mg-montmorillonite particles in the presence and absence of added magnesium ions, the general shape of Mg-montmorillonite aggregates with excess of Mg^{2+} ions is more ordered than the Na-counterpart. Such aggregates have been described as the *book house structure*,[48,49] which has fewer cavities inside than the *card house structure*.

All results so far obtained from this work indicate that the electrooptic method, i.e., reversing-pulse electric birefringence, is useful to study large colloidal particles. Since this method is very sensitive to change of the electrical, optical, and hydrodynamic properties, we could quantitatively estimate the effect of concentration of clay particle, and the ionic strength and valence of added counterion on the colloidal properties. Moreover, we could make some important inferences on the shape of aggregates, i.e., *card house structure* and *book house structure*.[48,49] We believe that these results provide basic information for diverse applications of the clay minerals. The reversing-pulse generator reported in this paper can apply electric pulses to clay dispersions only to about 0.5 kV cm^{-1}. The present electron microscopic photograph, however, shows that the Na-montmorillonite sample is considerably polydisperse regarding distribution of particle sizes. To study such a particle size distribution, the birefringence measurement must be extended to much higher fields, where smaller size particles can also be oriented. In this case, the measured data must be analyzed with the SUSID orientation function, which takes into account the size distribution.[35] We shall treat this problem of polydispersity with an improved pulse generator in the near future.

Conclusions

The new reversing-pulse generator was designed and constructed with the following specifications: the maximum applied voltage is limited to 300 V, but the long pulse duration is continuously variable up to 1.2 s. The improved driver amplifier and final discharge unit deliver either a single square-wave pulse or double pulses of opposite polarities with very fast time constants to high ionic strength solutions without appreciable voltage sagging. The new pulse generator uses MOS-FET transistors with a high electric-current endurance as the switching element. With the present pulse generator, the electric field orientation of both large particles, such as clay, and small macromolecules, such as DNA fragments,[50] would become feasible under physiological conditions.

The present RPEB measurements of montmorillonite particles dispersed in aqueous media revealed that the Na-montmorillonite particle possesses no *permanent electric dipole moment* and that the observed sign inversion of the steady-state electric birefringence is not due to the *permanent dipole moment* but to the *counterion-induced polarization*. Over the entire range of particle concentrations, Na-montmorillonite particles form no aggregates, but there is the interparticle interaction between the electric double layers of particles in $c > 0.029$ g dm^{-3}. Over the entire of ionic strength range, the sodium ions in aqueous media are primarily adsorbed onto the cation-exchangeable sites of Na-montmorillonite, which forms aggregates with the *card house structure* at higher ionic strengths. The field dependence of $\langle\tau\rangle_{EB}$ behaved differently above and below the sign inversion point. The change of the orientational axis probably occurs at this point from the out-of-plane to in-plane direction of a disk. The Mg-montmorillonite particles form aggregates with the *book house structure*, whose orientation function could be described neither by the YTS theory for transient RPEB signals nor by the PD-SUSID orientation function for the disklike particle. The origin of these anomalies may be attributed qualitatively to complex aggregate formation.

Acknowledgment. We thank Prof. T. Kitagawa, Faculty of Science of Hiroshima University, for kindly taking electron micrographs of our samples and his advice on the montmorillonite properties. This work partly supported by the Sasagawa Scientific Research Grant from The Japan Science Society. This work was in part supported by Grant-in-Aid for Developmental Scientific Research (B) No. 0655403 from the Ministry of Education, Science and Culture, Japan.

References and Notes

(1) Fredericq, E.; Houssier, C. *Electric Dichroism and Electric Birefringence*; Clarendon Press: Oxford, 1973.
(2) Stoylov, S. P. *Colloid Electro-Optics: Theory, Techniques, Applications*; Academic Press: New York, 1991.
(3) O'Konski, C. T.; Zimm, B. H. *Science* **1950**, *111*, 113.
(4) Benoit, H. *Ann. Phys. (Paris)* **1951**, *6*, 561.
(5) Tinoco, I., Jr. *J. Am. Chem. Soc.* **1957**, *79*, 4336.
(6) O'Konski, C. T.; Yoshioka, K.; Orttung, W. H. *J. Phys. Chem.* **1959**, *63*, 1558.
(7) O'Konski, C. T.; Bergmann, K. *J. Chem. Phys.* **1962**, *37*, 1573.
(8) Shah, M. J. *J. Phys. Chem.* **1963**, *67*, 2215.
(9) Charney, E.; Milstien, J. B.; Yamaoka, K. *J. Am. Chem. Soc.* **1970**, *92*, 2657.
(10) Kobayasi, S.; Ikegami, A. *Biopolymers* **1975**, *14*, 543.
(11) Yamaoka, K.; Ueda, K. *J. Phys. Chem.* **1982**, *86*, 406.
(12) Yoshioka, K.; Fujimori, M.; Yamaoka, K.; Ueda, K. *Int. J. Biol. Macromol.* **1982**, *4*, 55.
(13) Yamaoka, K.; Matsuda, K. *Macromolecules* **1981**, *14*, 595.
(14) Yamaoka, K.; Asato, M.; Matsuda, K.; Ueda, K. *Bull. Chem. Soc. Jpn.* **1984**, *57*, 1771.
(15) Yamaoka, K.; Yamamoto, S.; Ueda, K. *J. Phys. Chem.* **1985**, *89*, 5192.
(16) Yamaoka, K.; Ueda, K.; Kosako, I. *J. Am. Chem. Soc.* **1986**, *108*, 4619.
(17) Yamaoka, K.; Yamamoto, S.; Kosako, I. *Polym. J.* **1987**, *19*, 951.
(18) Yoshida, M.; Hayashi, M.; Kikuchi, K.; Watanabe, H. In *Dynamic Behavior of Macromolecules, Colloids, Liquid Crystals and Biological Systems by Optical and Electrooptical Methods*; Hirokawa Publ. Co.: Tokyo, 1989; pp 249−355.
(19) Khlebtsov, N. G.; Melnikov, A. G.; Bogatyrev, V. A. *J. Colloid Interface Sci.* **1991**, *146*, 463.
(20) Smith, K. L.; Fuller, G. G. *J. Colloid Interface Sci.* **1993**, *155*, 183.
(21) Yamaoka, K.; Fukudome, K.; Matsumoto, S.; Hino, Y. *J. Colloid Interface Sci.* **1994**, *168*, 349.
(22) Sasai, R.; Yamaoka, K. *J. Phys. Chem.* **1995**, *99*, 17754.
(23) Yamagishi, A.; Soma, M. *J. Phys. Chem.* **1981**, *85*, 3090.
(24) Yamaoka, K.; Sasai, R.; Ikuta, N. *Chem. Lett.* **1994**, 563.
(25) Yamaoka, K.; Tanigawa, M.; Sasai, R. *J. Chem. Phys.* **1994**, *101*, 1625.
(26) Yoshioka, K. In *Molecular Electro-Optics*; O'Konski, C. T., Ed.; Marcel Dekker: New York, 1978; Part 2, Chapter 17, pp 601−643.
(27) Yamaoka, K.; Fukudome, K. *J. Phys. Chem.* **1988**, *101*, 1625.
(28) Yamaoka, K.; Fukudome, K. *J. Phys. Chem.* **1990**, *94*, 6896.
(29) Yamaoka, K.; Fukudome, K.; Matsuda, K. *J. Phys. Chem.* **1992**, *96*, 7132.
(30) Yamaoka, K.; Matsuda, K. *Macromolecules* **1980**, *13*, 1558.
(31) Stellwagen, N. C. *Biopolymers* **1981**, *20*, 399.
(32) Stellwagen, N. C. *Biophys. Chem.* **1982**, *15*, 311.
(33) Matsuda, K.; Yamaoka, K. *Bull. Chem. Soc. Jpn.* **1982**, *55*, 69.
(34) Charney, E.; Yamaoka, K. *Biochemistry* **1982**, *21*, 834.
(35) Tanigawa, M.; Fukudome, K.; Yamaoka, K. *J. Sci. Hiroshima Univ. Ser. A* **1994**, *58*, 123.
(36) Yamaoka, K.; Kimura, M.; Okada, M. *Bull. Chem. Soc. Jpn.* **1992**, *65*, 129.
(37) Krămer, U.; Hoffmann, H. *Macromolecules* **1991**, *24*, 256.
(38) Soda, T.; Yoshioka, K. *Nippon Kagaku Zasshi* **1965**, *86*, 1019.
(39) Yoshioka, K. *J. Chem. Phys.* **1983**, *79*, 3482.
(40) Yamaoka, K.; Hino, Y. *Bull. Chem. Soc. Jpn.* **1989**, *62*, 251.
(41) Yamaoka, K.; Yamamoto, S.; Kimura, M.; Kosako, I. *Polym. J.* **1991**, *23*, 1443.
(42) Yamaoka, K.; Ueda, K. *Chem. Lett.* **1983**, 545.
(43) Tinoco, I., Jr. *J. Am. Chem. Soc.* **1955**, *77*, 4486.
(44) Pörschke, D.; Obst, A. *Rev. Sci. Instrum.* **1991**, *62*, 818.
(45) Tinoco, I., Jr.; Yamaoka, K. *J. Phys. Chem.* **1959**, *63*, 423.
(46) In Table 1 of our previous paper,[22] the value of $(\delta_{st}/cd)_\infty$ should be corrected from −15.7 to −15.0, and footnote (a) should read as "This value is given by $(\delta d^{-1})(-2/c)$, where ...". The term "intrinsic" in p 17760 (subheading and line 16 from bottom) should read as "limiting".
(47) Perrin, F. *J. Phys. Radium* **1934**, *5*, 497.
(48) *Clay Handbook*; Giho-do Co., Ltd.: Tokyo, 1976.
(49) Chernia, Z.; Gill, D.; Yariv, S. *Langmuir* **1994**, *10*, 3988.
(50) Tanigawa, M. *J. Sci. Hiroshima Univ. Ser. A* **1995**, *59*, 1.

JP961525+